

Article

Water Uptake in PHBV/Wollastonite Scaffolds: A Kinetics Study

Renata G. Ribas ^{1,*} , Thaís L. A. Montanheiro ¹ , Larissa S. Montagna ²,
Renata Falchete do Prado ³ , Ana Paula Lemes ², Tiago M. Bastos Campos ¹ and Gilmar P. Thim ¹

¹ Laboratory of Plasmas and Processes, Technological Institute of Aeronautics, Praça Marechal Eduardo Gomes, 50—Vila das Acácias, São José dos Campos SP 12228-900, Brazil

² Technology Laboratory of Polymers and Biopolymers, Federal University of São Paulo, Talim, 330—Vila Nair, São José dos Campos SP 12231-280, Brazil

³ Department of Dental Material and Prosthodontics, São Paulo State University, São José dos Campos SP 12245-000, Brazil

* Correspondence: rguimaraes42@gmail.com; Tel.: +55-(12)-3947-5958/98228-1574

Received: 29 May 2019; Accepted: 10 July 2019; Published: 16 July 2019



Abstract: Poly(3-hydroxybutyrate-co-3-hydroxyvalerate) (PHBV) is a widely studied polymer and it has been found that porous PHBV materials are suitable for substrates for cell cultures. A crucial factor for scaffolds designed for tissue engineering is the water uptake. This property influences the transport of water and nutrients into the scaffold, which promotes cell growth. PHBV has significant hydrophobicity, which can harm the production of cells. Thus, the addition of α -wollastonite (WOL) can modify the PHBV scaffold's water uptake. To our knowledge, a kinetics study of water uptake of α -wollastonite phase powder and the PHBV matrix has not been reported. In this work, PHBV and WOL, (PHBV/WOL) films were produced with 0, 5, 10, and 20 wt % of WOL. Films were characterized, and the best concentrations were chosen to produce PHBV/WOL scaffolds. The addition of WOL in concentrations up to 10 wt % increased the cell viability of the films. MTT analysis showed that PHBV/5%WOL and PHBV/10%WOL obtained cell viability of 80% and 98%, respectively. Therefore, scaffolds with 0, 5 and 10 wt % of WOL were fabricated by thermally induced phase separation (TIPS). Scaffolds were characterized with respect to morphology and water uptake in assay for 65 days. The scaffold with 10 wt % of WOL absorbed 44.1% more water than neat PHBV scaffold, and also presented a different kinetic mechanism when compared to other samples. Accordingly, PHBV/WOL scaffolds were shown to be potential candidates for biological applications.

Keywords: poly(3-hydroxybutyrate-co-3-hydroxyvalerate); wollastonite; composites; scaffolds; kinetics; water absorption

1. Introduction

In the last few decades, life expectancy has increased, along with an increase in health problems like osteoporosis and osteoarthritis [1–3]. These problems make it necessary to develop materials that can be used for bone repair and that can interact with biological systems. Poly(3-hydroxybutyrate-co-3-hydroxyvalerate) (PHBV) is a polyester from the polyhydroxyalkanoates (PHA) family synthesized by bacteria, which has been widely studied for tissue regeneration because it is a natural, biocompatible and nontoxic polymer [4–7]. However, PHBV is brittle and has low mechanical properties, so, efforts have been made to reinforce this matrix, for example by incorporating natural fibers, glass fibers, and carbon nanotubes, among others [8–12]. However, PHBV has a hydrophobic nature, which is not ideal for cell attachment and proliferation [13].

Some ceramic materials such as hydroxyapatite, β -tricalcium phosphates, bio-glasses and silicates, can interact with biological environments, chemically integrating with surrounding bone tissue *in vivo*. They are known as “bioactive” and numerous studies have utilized these materials to improve polymers’ mechanical properties [14,15]. One of these bioactive ceramic materials is wollastonite (WOL).

WOL is a highly bioactive calcium silicate (CaSiO_3) [16,17]. When in contact with body fluids, this silicate promotes Ca^{2+} ions liberation with the formation of Si-OH bonds on their surface. These Ca^{2+} ions precipitate along with phosphate ions present in the body fluid, inducing a superficial apatite layer. In the degradation, silica ions stimulate host cells to produce bone tissue [18]. Therefore, tissue formation and collagen mineralization occur due to apatite nucleation on the material surface [19].

The incorporation of WOL (or nano-wollastonite) into polyethylene [20], polycaprolactone [21] and even PHBV [22–24] has already been reported. All of these works have demonstrated that the incorporation of WOL into polymer matrix has potential application for bone substitution, due to the formation of apatite on the material, bioactivity and even differentiation of cells into osteoblasts. Additionally, other works have shown that incorporating WOL into a polymeric matrix results in a composite with better mechanical properties. Kotela et al. [21] reported significant improvement in the mechanical properties of polycaprolactone scaffolds with the addition of small amounts of nano-wollastonite.

Another essential factor in scaffolds designed for tissue engineering is the water uptake, since this property will influence the transport of water and nutrients into the scaffold, besides helping with the storage of growth factors [25,26]. Adding WOL to PHBV scaffolds may cause changes in the final material’s hydrophilicity, and consequently, in the water uptake due to PHBV’s significant hydrophobicity [27]. Besides that, the addition of WOL can promote changes in the local environment, neutralizing the acidic residues of PHBV degradation [25].

To our knowledge, a kinetics study of the water uptake of α -wollastonite phase powder and the PHBV matrix has not been reported. In this work, PHBV films were prepared by the solvent casting method with 5, 10, and 20 wt % of WOL. A complete characterization of the films was performed, and then scaffolds were produced with the best-observed conditions, to evaluate their absorption properties in water.

2. Materials and Methods

2.1. Materials

Poly(3-hydroxybutyrate-co-3-hydroxyvalerate) was provided by PHB Industrial, Brazil, with 3.76 mol% of hydroxyvalerate units and an average molecular weight (M_w) of $187.000 \text{ g mol}^{-1}$. Chloroform P.A. from Alphatec and Dioxane 1,4 P.A. from Synth (Brazil) were used as solvents. WOL was prepared by the sol-gel method [28]. Sodium metasilicate solution was mixed with ionic change resin (IR 120-Rohm and Haas) to form orthosilicic acid ($\text{Si}(\text{OH})_4$). In proportion, orthosilicic acid and calcium chloride were mixed with ethylene glycol 20% in volume. After that, the solution was left to dry for 24 h at $80 \text{ }^\circ\text{C}$. Finally, the dried powder was calcined first at $600 \text{ }^\circ\text{C}$ for 5 h to remove all the organic compounds and then calcined at $900 \text{ }^\circ\text{C}$ for another 5 h [25].

2.2. Production of PHBV/WOL Films

Films of PHBV/WOL were prepared using the solution-casting method. First, PHBV mass was solubilized in chloroform, and then WOL was added to the solution and the mixture was dispersed using a Hielscher UP200S (200 W, 24 kHz; Hielscher Ultrasonics GmbH, Teltow, Brandenburg, Germany) ultrasonic processor with 40% of amplitude for 2 min. The concentration of WOL utilized to prepare the samples PHBV, PHBV/5%WOL, PHBV/10%WOL and PHBV/20%WOL were 0, 5, 10 and 20 wt %, respectively. The resulting volume was poured onto Petri plates, and the mixtures were allowed to stand overnight, covered with aluminum paper to guarantee a slow evaporation. Films were obtained after the complete evaporation of chloroform at room temperature.

2.3. Production of PHBV/WOL Scaffolds

For neat PHBV scaffolds, PHBV was solubilized in dioxane at 70 °C under stirring for 2 h to give a 6% w/v solution. The solution was sonicated in a Hielscher UP200S ultrasonic processor (200 W, 24 kHz; Hielscher Ultrasonics GmbH, Teltow, Brandenburg, Germany) with 40% of amplitude for 2 min and then 5 mL aliquots of the solutions were poured into flasks and cooled down to −43 °C for 30 min. Samples were freeze-dried at −86 °C for 24 h in a Labconco Free Zone 2.5 Plus Lyophilizer (Labconco Corporation, Kansas City, MO, USA). For PHBV/WOL scaffolds, the desired amount of WOL to give 5 and 10 wt % concentrations were added to PHBV solubilized in dioxane and the same methodology used for neat PHBV scaffolds was followed. Scaffolds of neat PHBV, PHBV/WOL 5 wt %, and PHBV/WOL 10 wt % were labeled PHBV-S, PHBV/5%WOL-S, and PHBV/10%WOL-S, respectively.

2.4. Characterization

2.4.1. X-ray Diffraction (XRD)

Phase composition of WOL was analyzed by X-ray diffraction (PANalytical EMPYREAN, Malvern Panalytical Ltd, Malvern, UK) with Cu-K α radiation ($\lambda = 1.5406 \text{ \AA}$) in the 2θ range 20–55° at a scan rate of 0.6 s/step. The operating current and voltage were set at 40 mA and 40 kV, respectively.

2.4.2. Zeta Potential

The zeta potential value of WOL was obtained using dynamic light scattering equipment, Beckman Coulter Delsa Nano (Beckman Coulter, Brea, CA, USA). WOL powder was dispersed in deionized water (pH 5), and the measurements were performed at 25 °C at an angle of 15°. To calculate the zeta potential from mobility values, the Smoluchowski equation was used, with values of refractive index, dielectric constant, and viscosity of water at 25 °C.

2.4.3. Field Emission Gun—Scanning Electron Microscopy (FEG-SEM) and Scanning Electron Microscopy (SEM)

The morphology of WOL powder was analyzed by Field Emission Gun—Scanning Electron Microscopy (FEG-SEM) (MIRA3—TESCAN, Brno, Czech Republic) operating at 5 kV. The powder was fixed on aluminum stubs and covered with gold. The cryogenic fracture surface morphology of the films and scaffolds were observed by scanning electron microscopy (SEM) using an Inspect S50—FEI Company[®] microscope (FEI Company, Hillsboro, OR, USA), with detectors of secondary electrons mode (SE) and an accelerating voltage of 7.5 kV. The samples were cryogenically fractured, fixed on aluminum stubs and covered with gold.

2.4.4. Fourier Transform Infrared Spectroscopy (FT-IR)

FT-IR spectra were recorded on a Frontier spectrometer (PerkinElmer, Waltham, MA, USA), equipped with a universal attenuated total reflection (UATR) accessory. Each spectrum was acquired in transmittance mode by the accumulation of 32 scans with a range of 4000–400 cm^{-1} .

2.4.5. Raman Spectroscopy

Raman analyses was carried out using a LabRam HR Evolution spectrometer (HORIBA Scientific, Kyoto, Japan), coupled to an optical microscope with Nd:Yag laser (532 nm).

2.4.6. Contact Angle

Static contact-angle measurements of the scaffolds were examined in air at room temperature using a Ramé-Hart Model 500 (Ramé-Hart Instrument Co., Succasunna, NJ, USA). Contact-angle values were automatically calculated using DSA software. Measurements were made by dropping 10 mL of water on the film surface. Contact-angle values were obtained using an average of five measurements.

2.4.7. Cell Viability

Samples were cut into cylinders measuring 4 mm × 0.4 mm, then were transferred to 96-well plates. Dentistry metal matrix bands were used to fix the samples on the bottom of the well to avoid floating when inserted in culture medium. Plates were covered and exposed to ultraviolet rays for 15 min. Then, the set was turned and exposed for another 15 min. Human Dental Pulp Stem Cells (DPSC Lonza, Lonza Group, Basel, Switzerland) (density 8 × 10³ cells) were plated over samples in each well (n = 3 samples per group) using DMEM (Gibco, Thermo Fisher Scientific, Carlsbad, CA, USA) supplemented with 10% Fetal Bovine Serum (FBS Gibco, Thermo Fisher Scientific) and 5 mL of penicillin and streptomycin (PEN-STREP 100000 un-10 mg/mL, Sigma Aldrich, Darmstadt, Germany).

After being cultured for 3 days, culture medium was replaced by MTT solution [3-(4,5-dimethylthiazol-2-yl)-2,5-diphenyltetrazolium bromide] (5 mg/mL PBS, Sigma Aldrich). The solution was added and the cells were incubated at 37 °C, for 1 h to form purple formazan crystals [29,30]. The cytotoxicity assay was performed using bottom of well as a control. After incubation, supernatant was removed and samples were washed with PBS, followed by the addition of isopropanol acid (0.04 mol/L HCL in isopropanol) to each well in order to dissolve the formazan crystals. Colorimetric analysis was performed with an EL808IU Spectrophotometer (Biotek Instruments, Winooski, VT, USA) at 570 nm. Data was normalized using the control group as 100%, and expressed as percentage.

2.4.8. Water Uptake

Dry scaffolds (W_d) were immersed into distilled water for 65 days at ambient temperature. At selected intervals, they were removed from the water, blotted dry on filter paper to remove excess water, weighed and returned to the water. The weighed scaffolds were denominated (W_w). The water uptake was obtained using Equation (1):

$$WU (\%) = \frac{(W_w - W_d)}{W_d} \times 100 \quad (1)$$

3. Results

3.1. X-ray Diffraction

X-ray diffraction was carried out to confirm the wollastonite phase obtained by the sol-gel method. Figure 1 shows the diffractogram of the WOL powder used to produce both scaffolds and composites films. As observed, only the peaks of the α -wollastonite (also known as pseudo-wollastonite) phase are present (PDF#740874). This diffractogram proves that the α -wollastonite phase is pure, and no other phases were formed in the synthesis.

Most studies reported in the literature prepared pure α -wollastonite at 1125 °C or above [16,31,32]. A common route to obtain α -wollastonite is to prepare it by solid-state reaction, as reported in the work of Hossain and Roy [31]. In this study, the authors prepared pseudo-wollastonite phase utilizing eggshell (~99% CaO) and rice husk ash (~93% SiO) as precursors. Powders were wet ball-milled in water and then, the mixture was dried at 110 °C and calcined at 1000, 1100, 1150 and 1200 °C. The α -wollastonite phase only appeared in samples calcined at 1150 and 1200 °C. However, both presented parawollastonite (PDF#3-1460) as a secondary phase.

Wang et al. [32] synthesized pure α -wollastonite phase by using the sol-gel process, utilizing calcium nitrate (Ca(NO₃)₂·4H₂O) and tetraethyl orthosilicate (TEOS) as precursors, and calcining the WOL xerogel at 1150 °C, the pseudo wollastonite was completely formed.

Therefore, the methodology reported here was efficient for producing WOL with lower temperatures and to obtain the pure α phase.

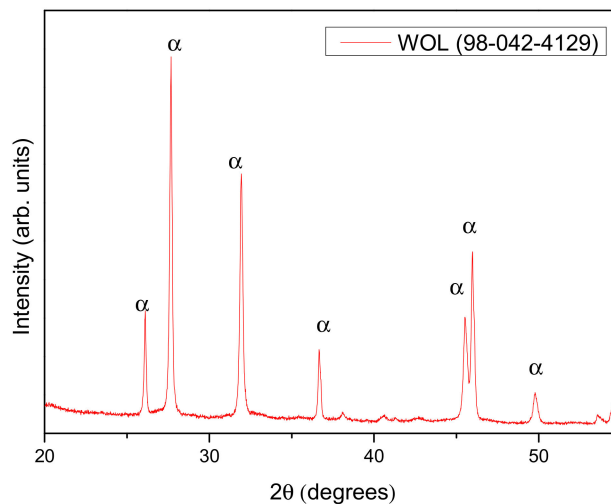


Figure 1. X-ray diffraction pattern of α -wollastonite (WOL) synthesized.

3.2. Zeta Potential

Measurement of the zeta potential was performed to estimate the surface charge of WOL powder [33]. The dispersion was performed in deionized water. A value of -29 mV was found. This may be considered a “quasi” stable suspension, since colloidal particles are considered stable when they have a zeta potential of magnitude greater than ± 30 mV [34] in these conditions. The negative zeta potential may be attributed to the presence of silanol groups present on the surface of WOL and will be discussed further.

3.3. Field-Emission Scanning Electron Microscopy (FEG-SEM)

The morphology of WOL powder was investigated by FEG-SEM and representative micrographs are shown in Figure 2. WOL powder presents particles with numerous interconnected pores, which can be found all over the sample. This is an important characteristic for scaffolds for bone substitution since this property could influence the transport of nutrients to cells for growth [25,26].

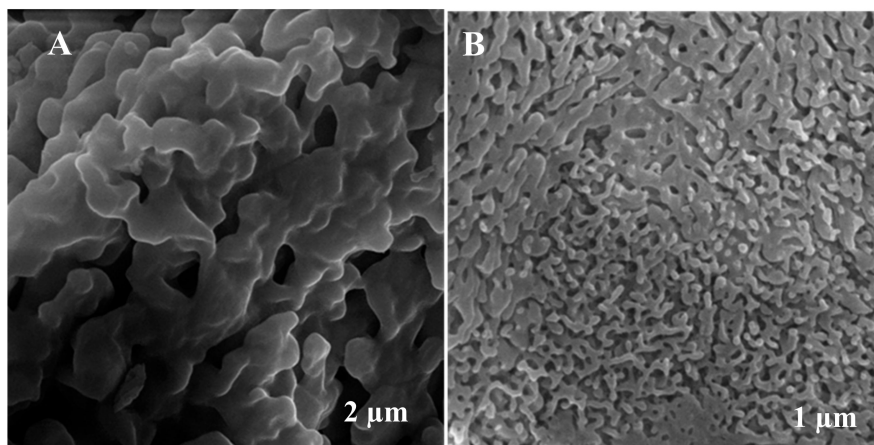


Figure 2. FEG-SEM micrographs of powder WOL. (A) 40000 \times and (B) 20000 \times .

Similar morphology was reported in a previous work by Paluszkiewicz et al. [35] for α -wollastonite; however, there was less porosity than in the sample shown in Figure 2. This distinction is probably due to different methodologies employed to produce α -wollastonite. They sintered the sample at 1200 $^{\circ}\text{C}$, whereas in this work, wollastonite was produced at 900 $^{\circ}\text{C}$.

3.4. Raman Spectroscopy

Raman spectra of WOL, neat PHBV, PHBV/5%WOL, PHBV/10%WOL, and PHBV/20%WOL are shown in Figure 3, where it can be observed that the spectra of neat PHBV is quite similar to the spectrum of PHBV/WOL films. The difference is the peaks related to WOL, especially peaks at 366 (Ca-O stretch), at 577 (O-Si-O bend), and at 977 (Si-O br stretch) cm^{-1} [36]. Table 1 presents the peaks of wollastonite and PHBV reported in previous literature [36,37]. The peaks of WOL are more expressive in the samples with more proportionality of the silicate and could not be observed in the PHBV/5% WOL.

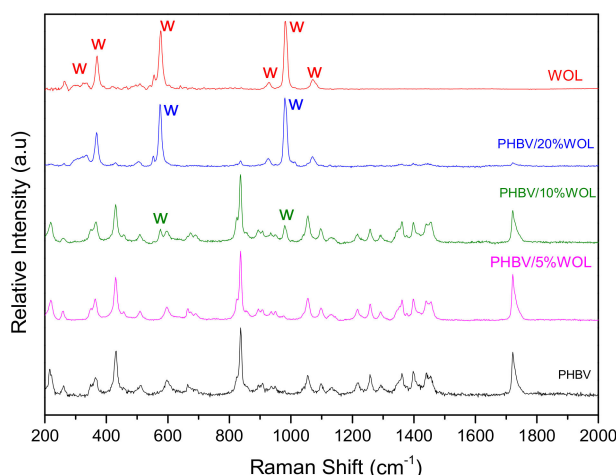


Figure 3. Raman spectra of WOL powder and neat poly(3-hydroxybutyrate-co-3-hydroxyvalerate) (PHBV), PHBV/5%WOL, PHBV/10%WOL and PHBV/20%WOL films.

Peaks of PHBV in the spectra of PHBV/WOL films have no displacement, which means that there is no change in the chemical structure of the polymeric matrix. There are no other different peaks apart from those observed, either in neat PHBV or in WOL spectra, which means that PHBV/WOL had no parallel reactions.

3.5. FT-IR Spectroscopy

FT-IR spectra of WOL powder, neat PHBV, PHBV/5%WOL, PHBV/10%WOL, and PHBV/20%WOL films are shown in Figure 4. Table 2 list all the WOL and PHBV bands reported in the literature [35,38–40]. Two of the characteristic bands for α -wollastonite (714 and 922 cm^{-1}) can be observed in all PHBV/WOL films, confirming the presence of WOL in the composite films. However, some bands of the silicate and PHBV are overlapped, making it difficult to achieve a precise analysis. Due to the small quantities of WOL incorporated in the films, and to the possible covering of WOL particles by PHBV matrix, other bands have signals too low to be identified.

Kolesov and Geiger [39] investigated the behavior of H_2O in FT-IR and Raman spectra in zeolites natrolite ($\text{Na}_{16}[\text{Al}_{16}\text{Si}_{24}\text{O}_{80}]\cdot 16\text{H}_2\text{O}$) and scolecite ($\text{Ca}_8[\text{Al}_{16}\text{Si}_{24}\text{O}_{80}]\cdot 24\text{H}_2\text{O}$). They realized that FT-IR spectra enabled an understanding of inner surface water molecule behavior in microporous silicates and the behavior of hydrogen bonding. They determined that the band located at 1636 cm^{-1} corresponds to the bending mode of water. Abadleh and Grassian [41] carried out a FT-IR study of water adsorption on aluminum oxide surfaces. They also assigned the band at 1645 cm^{-1} to liquid water adsorbed on the surface of the samples.

Therefore, the band positioned at $\sim 1620 \text{ cm}^{-1}$ in the spectra of WOL was probably the bending mode of H_2O [38] and the band around 960 cm^{-1} was assigned to the Si-OH bond of the silanol group [42]. These sites of water absorption are due to the silanol groups and are in agreement with zeta potential results.

The PHBV/WOL composites spectra do not present the band at 1620 cm^{-1} as WOL spectrum, which occurs probably because the polymeric chains embed the wollastonite particles. Though the presence of these particles is not reflected in the FT-IR spectrum, WOL particles are indeed incorporated in the matrix, which leads to an increase in water adsorption, which is proportional to the increase in WOL content.

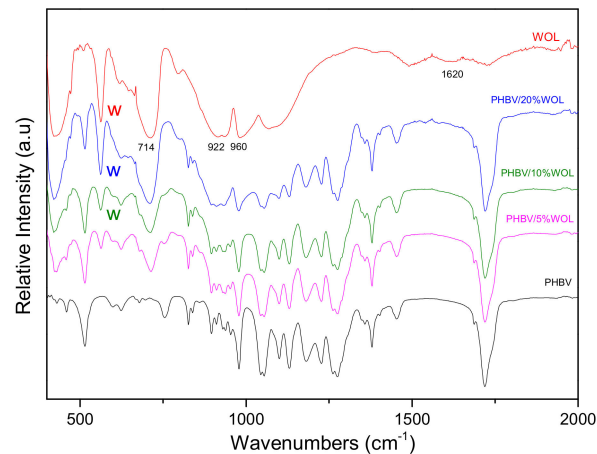


Figure 4. FT-IR spectra of WOL powder and neat PHBV, PHBV/5%WOL, PHBV/10%WOL and PHBV/20%WOL films.

3.6. SEM Micrographs

Figure 5 shows the morphological characterization of the cryogenic fracture surface of neat PHBV, PHBV/5%WOL, PHBV/10%WOL, and PHBV/20%WOL composites films. Figure 5A corresponds to the fracture surface of neat PHBV. Figure 5B–D presents the surface fracture morphology of PHBV/5%WOL, PHBV/10%WOL, and PHBV/20%WOL, respectively. PHBV/5%WOL and PHBV/10%WOL presented uniformly dispersed WOL particles, good interfacial adhesion and no agglomeration. However, PHBV/20%WOL shows the presence of agglomerated WOL particles, and provides evidence of the poor interaction between them and the matrix, perhaps due to the difficulty of dispersing the large content of particles in the PHBV matrix.

Bheemaneni et al. [43] prepared poly(butylene adipate-co-terephthalate) (PBAT)/WOL with 0 to 7 wt % of WOL by using the melt blending method. The authors observed that the highest concentrations of WOL (5 and 7 wt %) presented agglomerations and low adhesion with the PBAT matrix. Thus, the present work obtained PHBV/WOL films by the solution-casting method, which showed satisfactory dispersion of 5 and 10 wt % concentrations of WOL in the PHBV matrix. Therefore, due to the good interaction and dispersion of the 5 and 10 wt % WOL content in the PHBV matrix, these two concentrations were chosen to prepare scaffolds, labeled PHBV-S, PHBV/5%WOL-S, and PHBV/10%WOL-S.

Figure 6 shows a SEM micrograph of the fracture surface of neat PHBV-S, PHBV/5%WOL-S, and PHBV/10%WOL-S composites' scaffolds. Figure 6A shows the fracture surface morphology of neat PHBV, which exhibits a macroporous structure with interconnected open pores distributed across the macroporous walls. Figure 6B,C correspond to the composites PHBV/5%WOL-S and PHBV/10%WOL-S, respectively, and show a similar morphology to neat PHBV, and a uniform morphological surface with a similar macroporous structure compared to the neat PHBV scaffold. The different content of WOL particles are dispersed homogeneously in the scaffolds.

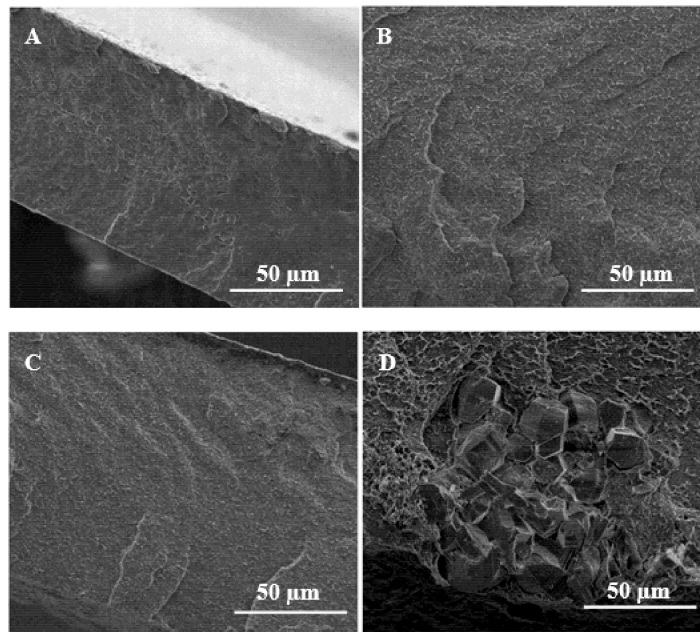


Figure 5. SEM micrograph of fracture surface of the samples in films forms: neat PHBV (A), PHBV/5%WOL (B), PHBV/10%WOL (C) and PHBV/20%WOL (D) with magification of 2000×.

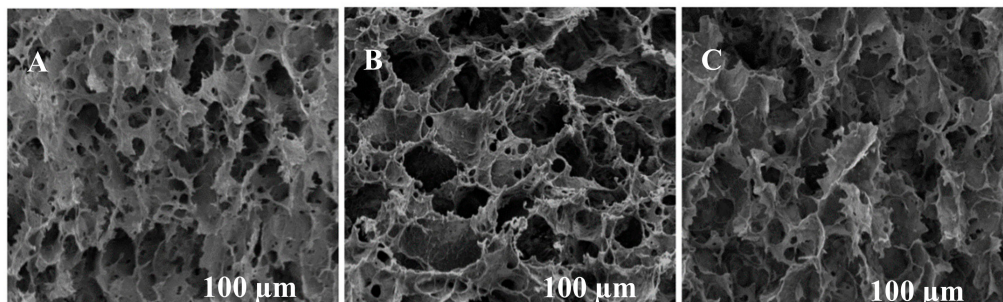


Figure 6. SEM micrograph of fracture surface of scaffolds: neat PHBV (A), PHBV/5% WOL-S (B), PHBV/10% WOL-S (C) with 1000x magnification.

Li et al. [23] obtained PHBV/WOL scaffolds with 20 and 40 wt % of WOL by a compression molding, thermal processing, and salt particulate leaching method. In SEM micrographs, the authors observed that when these concentrations were used, some WOL particles aggregate, although the macroporous structure was still maintained.

3.7. Contact Angle

The contact angle of the films was obtained to evaluate the influence of WOL in the hydrophilicity of PHBV. Figure 7 shows the average result and the standard deviation.

The average value of the contact angle was not affected by the addition of 5 and 10 wt % of WOL. WOL is a hydrophilic material [44,45], which may contribute to increasing the hydrophilicity of the PHBV matrix over time. However, WOL is probably not exposed on the surface of the films but embedded by the PHBV matrix. Then, the contact angle would remain unchanged.

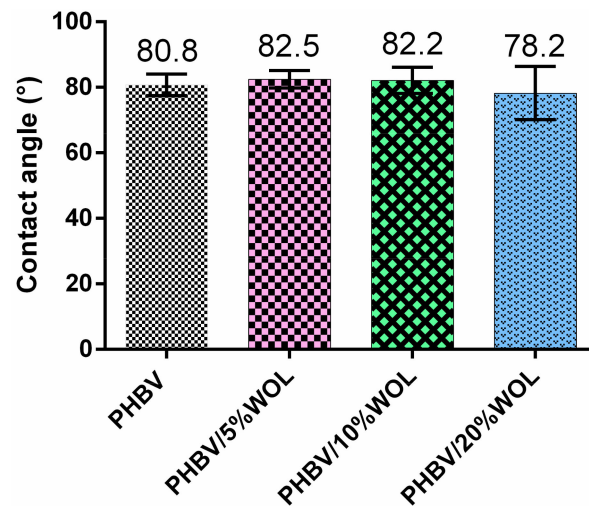


Figure 7. Contact angle values of neat PHBV, PHBV/5%WOL and PHBV/10%WOL films.

3.8. Cell Viability

The effect in cell viability of adding WOL into PHBV films was evaluated by MTT analysis. WOL is a non-cytotoxic bioceramic used as reinforcement for different polymeric matrices [10,43,44]. MTT analysis data is shown in Figure 8. PHBV/5%WOL and PHBV/10%WOL had a cell viability of 80% and 98%, respectively; considerably higher when compared to 52% of neat PHBV film. However, PHBV/20%WOL had a decrease in cell viability to 48%.

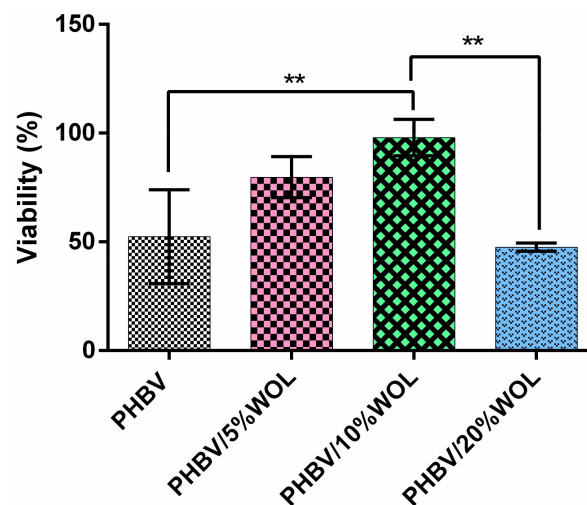


Figure 8. Human dental pulp stem cells proliferation on PHBV, PHBV/5%WOL, PHBV/10%WOL, and PHBV/20%WOL% films after 3 days. Results are given as mean \pm SD (n = 3). One-way ANOVA, significance levels: ** $p < 0.01$.

Bheemaneni et al. [43] showed that introducing 3 and 5 wt % wollastonite into poly(butylene adipate-co-terephthalate) (PBAT) matrix improved cell activity compared to neat PBAT. However, when they incorporated 7 wt %, the viability decreased. The authors attributed this reduction to a diminished superficial area due to WOL agglomeration in higher concentrations.

A similar behavior was observed for the PHBV/20%WOL composites, which showed poorly dispersed WOL particles, reducing the superficial area, and consequently, the cell viability. When particles are not satisfactorily dispersed into the matrix, there is an absence of filler effect [43], justifying the lower biocompatibility obtained for the sample with higher WOL concentration.

3.9. Water Uptake

To evaluate water uptake, scaffolds were immersed in water for 65 days and their mass was measured at predefined times. Figure 9a shows the results of the percentage of water absorbed for samples PHBV-S, PHBV/5%WOL-S, and PHBV/10%WOL-S. The PHBV/10%WOL-S sample absorbed 44.1% and 28.3% more water than neat PHBV-S and PHBV/5%WOL-S, respectively. Moreover, the PHBV/10%WOL-S sample achieved absorption equilibrium at around 960 h, much earlier than PHBV/5%WOL-S and PHBV-S (1200 h). The presence of silanol groups in addition to the porous surface of WOL, induces the water absorption in the scaffolds.

To better evaluate the mechanism of water uptake, a kinetic study was carried out by fitting the experimental data to the pseudo-first-order, pseudo-second-order and diffusion intraparticle models. The first two equations represent a chemical mechanism of water absorption, whereas the third one is related to physical absorption [46]. The pseudo-first-order can be described by Equation (2) [47]:

$$\log(q_e - q_t) = \log q_e - \frac{k_1 t}{2.303} \quad (2)$$

where, q_t and q_e are the mass of the adsorbed water at time t and at equilibrium, respectively, and k_1 is the rate constant of pseudo first-order adsorption process. The constants q_e and k_1 can be graphically determined by the plot $\log(q_e - q_t)$ versus t , where the slope is related to k_1 and the intercept is $\log(q_e)$.

The pseudo-second-order model can mathematically be described by Equation (3) [47,48]:

$$\frac{t}{q_t} = \frac{1}{k_2 q_e^2} + \frac{t}{q_e} \quad (3)$$

where, k_2 is the pseudo-second-order rate constant and q_t and q_e were previously described. The constants of Equation (3) can be graphically determined by plotting t versus (t/q_t) : the slope is related to the value of q_e , and the intercept is related to k_2 .

The intra particle diffusion model can be expressed by Equation (4) [47,48]:

$$q_t = k_{in} t^{0.5} + C \quad (4)$$

where q_t is the mass of adsorbed water at time t , k_{in} is a kinetic constant, which is directly related to the intraparticle diffusion parameter, and C is the thickness of the boundary layer. The values of the parameters k_{in} and C can be determined by a plot of q_t versus $t^{0.5}$, where k_{in} is the slope and C is the intercept.

All three samples were tested against the three models to evaluate which one better fits. The graphic results are presented in Figure 9b–d for PHBV-S, PHBV/5%WOL-S and PHBV/10%WOL-S, respectively.

The calculated constants are shown in Table 3. The model that better fits for samples PHBV-S and PHBV/5%WOL-S is the interparticle diffusion model. Therefore, both samples have the same physical mechanism of water absorption, in which water molecules permeate the scaffolds through the pores. However, with 10 wt % of WOL, the mechanism changes to the pseudo-first-order model, in which water molecules are chemically attracted to silanol groups on the surface of WOL [42]. Only for this concentration, is the quantity of silanol enough to modify the kinetics, which explains why the PHBV/5%WOL-S sample presents R^2 so close for the three models, predicting the amounts of water that will be absorbed concerning the mass of any prepared scaffold.

Until 48 h of immersion, no significant differences in the mass gain were observed between the three scaffolds. This phenomenon probably occurs because polymeric chains embed the WOL particles, which is in accordance with previous results: (1) no 1620 cm^{-1} band was observed in FT-IR, and (2) the average value of the contact angle was not affected. Water may penetrate polymeric chains and reach WOL particles only after 48 h, which alters the adsorption mechanism of water uptake, as seen in Figure 9.

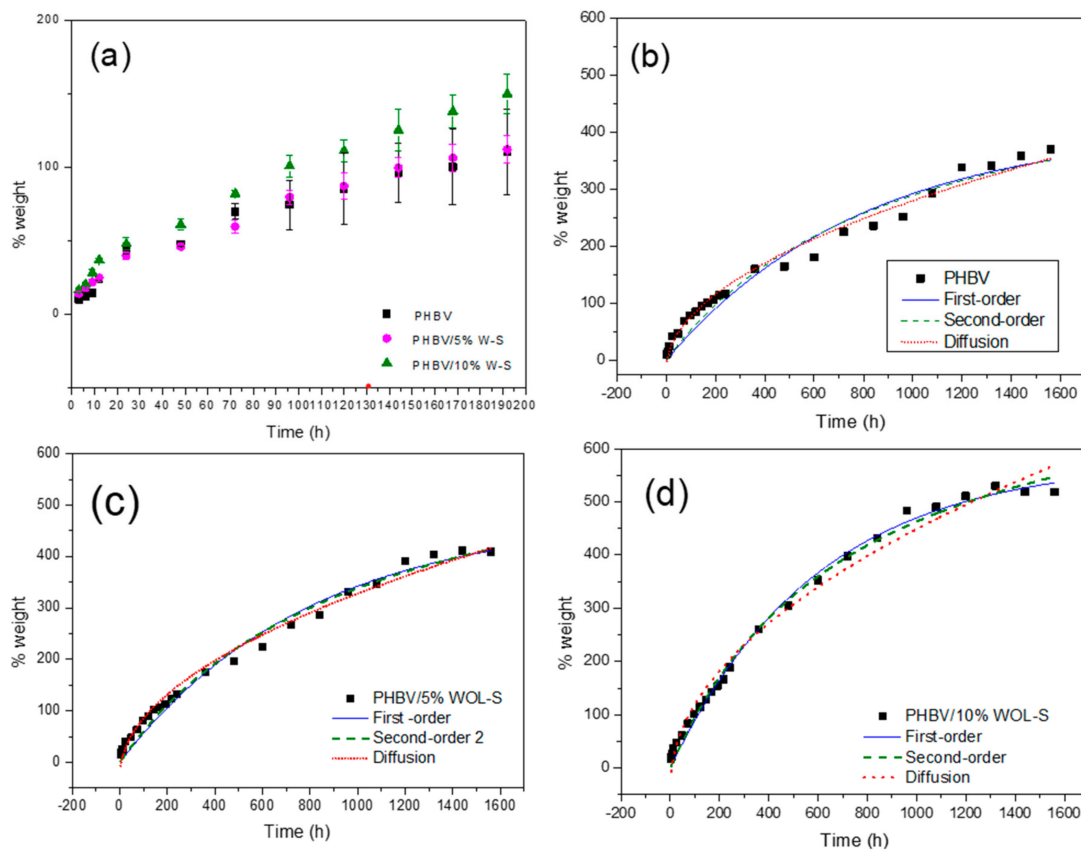


Figure 9. Results of water uptake (a) and kinetics fittings of PHBV (b), PHBV/5%WOL-S (c) and PHBV/10%WOL-S (d).

Table 1. The Raman assignments modes of WOL and PHBV.

Wollastonite		PHBV	
cm ⁻¹	Assignments	cm ⁻¹	Assignments
237, 337	Ca-O Stretch	678	γC=O
321, 337	Ca-O Stretch	693	γC=O
400, 412	Ca-O Stretch	840	νC-COO
485	O-Si-O bend	980	rCH ₃ , νC-C (C)
581	O-Si-O bend	1220	Helical conf. (C)
636	Si-O-Si bend	1262	Helical conf. (C)
688	Si-O-Si bend	1364	δCH, wCH ² , δ _s CH ₃
883	Si-O(br) stretch	1380	δ _s CH ₃
970	Si-O(br) stretch	1443/1458	δCH ₂ , δ _{as} CH ₃ (C)
997	Si-O(br) stretch	1725	νC=O (C)
1020	Si-O(br) stretch		
1044	Si-O(br) stretch		

Table 2. The FTIR active vibrational modes of the WOL and PHBV.

Wollastonite		PHBV	
cm ⁻¹	Assignments	cm ⁻¹	Assignments
~1640	Bending water	2975	Symmetric stretching of CH ₃ group
1092	Stretching bridging	2937	Asymmetric stretching of CH ₃ group
1072	Si-O(Si)	1725	Carbonyl stretching (C=O) of PHBV
~960	Si-OH		
985	Stretching non-bridging Si-O(Si)	1500–900	CH ₃ and CH vibrations and C-O-C and C-C stretching
938			
922			
714	Stretching bridging Si-O(Si)		

Table 3. Kinetics studies of water uptake to PHBV-S, PHBV/5%WOL-S and PHBV/10%WOL-S.

Samples	Pseudo First-Order Model			Pseudo Second-Order Model			Interparticle Diffusion Model	
	k ₁ (h ⁻¹)	q _e	R ²	k ₂ (h ⁻¹)	q _e	R ²	k _{in}	R ²
PHBV	1.25 × 10 ⁻³	408.65	0.96035	1.81 × 10 ⁻⁶	569.55	0.96707	9.39035	0.98374
PHBV/5%WOL	1.25 × 10 ⁻³	478.60	0.98229	1.40 × 10 ⁻⁶	689.05	0.98547	11.1993	0.98809
PHBV/10%WOL	1.68 × 10 ⁻³	578.22	0.99428	1.64 × 10 ⁻⁶	811.9	0.99381	15.26236	0.98577

4. Conclusions

In this work, films of PHBV/WOL composites with 0, 5, 10, and 20 wt % of WOL were prepared. X-ray diffractograms showed that the synthesized wollastonite was a pure α -wollastonite phase. The synthesis of this phase (pure α -wollastonite) at this low calcination temperature (900 °C) is not related in literature. Raman and FT-IR spectra showed that WOL does not interfere in the PHBV structure and had no secondary reactions. SEM images showed that WOL was uniformly dispersed into the PHBV matrix, had good interfacial adhesion and no agglomeration in PHBV/5%WOL and PHBV/10%WOL films. However, the PHBV/20%WOL sample presented agglomerates of WOL and poor particle-matrix interaction. Scaffolds of neat PHBV and PHBV/WOL showed opened-pore morphology, with interconnected pores, ideal for tissue regeneration. The addition of WOL in concentrations up to 10 wt % increased the cell viability of films. MTT analysis showed that PHBV/5%WOL and PHBV/10%WOL presented 80% and 98% cell viability, respectively. Water uptake was undoubtedly higher for PHBV/10%WOL-S, thus, kinetics studies were performed to better understand the mechanism of water absorption. PHBV/10%WOL-S presented different mechanisms for water uptake compared to neat PHBV-S and PHBV/5%WOL-S, which was attributed to the presence of silanol groups on the WOL surface. Only after 48 h, water may penetrate polymeric chains, which alters the adsorption mechanism of water up take. Thus, PHBV/WOL scaffolds are potential candidates for application as bone substitutes, as WOL improved water absorption, and consequently, will positively affect the transport of nutrients and promote cell adhesion. Additional studies are necessary to evaluate the effect of the mechanical properties of WOL in PHBV/WOL scaffolds.

Author Contributions: Conceptualization, R.G.R., T.L.A.M. and T.M.B.C.; methodology, R.G.R., T.L.A.M. and T.M.B.C.; software, R.G.R.; validation, R.G.R., T.L.A.M., T.M.B.C., G.P.T. and R.F.P.; formal analysis, R.G.R.; investigation, R.G.R., L.S.M. and R.F.P.; resources, A.P.L. and G.P.T.; data curation, R.G.R.; writing—original draft preparation, R.G.R.; writing—review and editing, R.G.R., T.L.A.M., L.S.M., T.M.B.C. and G.P.T.; visualization, R.G.R., T.L.A.M., T.M.B.C., G.P.T., A.P.L., and L.S.M.; supervision, G.P.T.; project administration, R.G.R., T.L.A.M. and T.M.B.C.; funding acquisition, G.P.T. and A.P.L.

Funding: The authors would like to thank the Brazilian Funding institutions CAPES and FAPESP (2017/27079-7; 2017/24873-4; 2018/12035-7) for the financial support and INPE for allowing us to use their MEV-FEG.

Conflicts of Interest: The funders had no role in the design of the study; in the collection, analyses, or interpretation of data; in the writing of the manuscript, or in the decision to publish the results.

References

1. Monma, H.; Ueno, S.; Kanazawa, T. Properties of hydroxyapatite prepared by the hydrolysis of tricalcium phosphate. *J. Chem. Technol. Biotechnol.* **1981**, *31*, 15–24. [[CrossRef](#)]
2. Johnell, O.; Kanis, J.A. An estimate of the worldwide prevalence and disability associated with osteoporotic fractures. *Osteoporos. Int.* **2006**, *17*, 1726–1733. [[CrossRef](#)] [[PubMed](#)]
3. Eisman, J.A.; Bogoch, E.R.; Dell, R.; Harrington, J.T.; McKinney, R.E.; McLellan, A.; Mitchell, P.J.; Silverman, S.; Singleton, R.; Siris, E. Making the first fracture the last fracture: ASBMR task force report on secondary fracture prevention. *J. Bone Miner. Res.* **2012**, *27*, 2039–2046. [[CrossRef](#)] [[PubMed](#)]
4. Montagna, L.S.; Montanheiro, T.L.D.A.; Machado, J.P.B.; Passador, F.R.; Lemes, A.P.; Rezende, M.C. Effect of Graphite Nanosheets on Properties of Poly (3-hydroxybutyrate-co-3-hydroxyvalerate). *Int. J. Polym. Sci.* **2017**, *2017*, 9. [[CrossRef](#)]
5. Lenz, R.W.; Marchessault, R.H. Bacterial polyesters: Biosynthesis, biodegradable plastics and biotechnology. *Biomacromolecules* **2005**, *6*, 1–8. [[CrossRef](#)] [[PubMed](#)]
6. Zinn, M.; Witholt, B.; Egli, T. Occurrence, synthesis and medical application of bacterial polyhydroxyalkanoate. *Adv. Drug Deliv. Rev.* **2001**, *53*, 5–21. [[CrossRef](#)]
7. Zhijiang, C.; Yi, X.; Haizheng, Y.; Jia, J.; Liu, Y. Poly(hydroxybutyrate)/cellulose acetate blend nanofiber scaffolds: Preparation, characterization and cytocompatibility. *Mater. Sci. Eng. C* **2016**, *58*, 757–767. [[CrossRef](#)]
8. Amaral Montanheiro, T.L.; Montagna, L.S.; Machado, J.P.B.; Lemes, A.P. Covalent functionalization of MWCNT with PHBV chains: Evaluation of the functionalization and production of nanocomposites. *Polym. Compos.* **2017**, *40*, 288–295. [[CrossRef](#)]
9. Jiang, L.; Huang, J.; Qian, J.; Chen, F.; Zhang, J.; Wolcott, M.P.; Zhu, Y. Study of Poly(3-hydroxybutyrate-co-3-hydroxyvalerate) (PHBV)/Bamboo Pulp Fiber Composites: Effects of Nucleation Agent and Compatibilizer. *J. Polym. Environ.* **2008**, *16*, 83–93. [[CrossRef](#)]
10. Li, H.; Zhai, W.; Chang, J. In vitro biocompatibility assessment of PHBV/Wollastonite composites. *J. Mater. Sci. Mater. Med.* **2008**, *19*, 67–73. [[CrossRef](#)]
11. Srithep, Y.; Ellingham, T.; Peng, J.; Sabo, R.; Clemons, C.; Turng, L.; Pilla, S. Melt compounding of poly (3-hydroxybutyrate-co-3-hydroxyvalerate)/nanofibrillated cellulose nanocomposites. *Polym. Degrad. Stab.* **2013**, *98*, 1439–1449. [[CrossRef](#)]
12. Ten, E.; Turtle, J.; Bahr, D.; Jiang, L.; Wolcott, M. Thermal and mechanical properties of poly(3-hydroxybutyrate-co-3-hydroxyvalerate)/cellulose nanowhiskers composites. *Polymer* **2010**, *51*, 2652–2660. [[CrossRef](#)]
13. Kouhi, M.; Fathi, M.; Prabhakaran, M.P.; Shamanian, M.; Ramakrishna, S. Enhanced proliferation and mineralization of human fetal osteoblast cells on PHBV-bredigite nanofibrous scaffolds. *Mater. Today Proc.* **2018**, *5*, 15702–15709. [[CrossRef](#)]
14. Li, W.; Noeaid, P.; Roether, J.A.; Schubert, D.W.; Boccaccini, A.R. Preparation and characterization of vancomycin releasing PHBV coated 45S5 Bioglass[®]-based glass–ceramic scaffolds for bone tissue engineering. *J. Eur. Ceram. Soc.* **2014**, *34*, 505–514. [[CrossRef](#)]
15. Kodal, M.; Erturk, S.; Sanli, S.; Ozkoc, G. Properties of Talc/Wollastonite/Polyamide 6 Hybrid Composites. *Polym. Compos.* **2015**, *6*, 739–746. [[CrossRef](#)]
16. De Aza, P.N.; Luklinska, Z.B.; Anseau, M.R.; Guitian, F.; De Aza, S. Bioactivity of pseudowollastonite in human saliva. *J. Dent.* **1999**, *27*, 107–113. [[CrossRef](#)]
17. De Aza, P.N.; Luklinska, Z.B.; Anseau, M.; Guitian, F.; De Aza, S. Morphological studies of pseudowollastonite for biomedical application. *J. Microsc.* **1996**, *182*, 24–31. [[CrossRef](#)]
18. Turnbull, G.; Clarke, J.; Picard, F.; Riches, P.; Jia, L.; Han, F.; Li, B.; Shu, W. 3D bioactive composite scaffolds for bone tissue engineering. *Bioact. Mater.* **2018**, *3*, 278–314. [[CrossRef](#)]
19. Xu, S.; Liu, J.; Li, Q. Mechanical properties and microstructure of multi-walled carbon nanotube-reinforced cement paste. *Constr. Build. Mater.* **2015**, *76*, 16–23. [[CrossRef](#)]

20. Rea, S.M.; Brooks, R.A.; Best, S.M.; Kokubo, T.; Bonfield, W. Proliferation and differentiation of osteoblast-like cells on apatite-wollastonite/polyethylene composites. *Biomaterials* **2004**, *25*, 4503–4512. [[CrossRef](#)]
21. Kotela, I.; Podporska, J.; Soltysiak, E.; Konsztowicz, K.J.; Blazewicz, M. Polymer nanocomposites for bone tissue substitutes. *Ceram. Int.* **2009**, *35*, 2475–2480. [[CrossRef](#)]
22. Li, H.; Chang, J. In vitro degradation of porous degradable and bioactive PHBV/wollastonite composite scaffolds. *Polym. Degrad. Stab.* **2005**, *87*, 301–307. [[CrossRef](#)]
23. Li, H.; Chang, J. Fabrication and characterization of bioactive wollastonite/PHBV composite scaffolds. *Biomaterials* **2004**, *25*, 5473–5480. [[CrossRef](#)] [[PubMed](#)]
24. Li, H.; Zhai, W.; Chang, J. Effects of wollastonite on proliferation and differentiation of human bone marrow-derived stromal cells in PHBV/Wollastonite composite scaffolds. *J. Biomater. Appl.* **2009**, *24*, 231–246. [[CrossRef](#)] [[PubMed](#)]
25. Zhu, H.; Shen, J.; Feng, X.; Zhang, H.; Guo, Y.; Chen, J. Fabrication and characterization of bioactive silk fibroin/wollastonite composite scaffolds. *Mater. Sci. Eng. C* **2010**, *30*, 132–140. [[CrossRef](#)]
26. Gobin, A.S.; Froude, V.E.; Mathur, A.B. Structural and mechanical characteristics of silk fibroin and chitosan blend scaffolds for tissue regeneration. *J. Biomed. Mater. Res. Part A* **2005**, *74*, 465–473. [[CrossRef](#)] [[PubMed](#)]
27. Rivera-Briso, A.; Serrano-Aroca, Á. Poly(3-Hydroxybutyrate-co-3-Hydroxyvalerate): Enhancement Strategies for Advanced Applications. *Polymers* **2018**, *10*, 732. [[CrossRef](#)] [[PubMed](#)]
28. Campos, T.M.B. Estudo da influencia do etileno glicol na cristalização da mulita obtida por método sol-gel. Master's Thesis, Instituto Tecnológico de Aeronáutica, São José dos Campos, São Paulo, Brazil, 2016.
29. Rosa, A.L.; Paulo, T.; Mario, T.J. Human alveolar bone cell proliferation, expression of osteoblastic phenotype, and matrix mineralization on porous titanium produced by powder metallurgy. *Clin. Oral Implant. Res.* **2009**, *20*, 472–481. [[CrossRef](#)]
30. Perez, D.; Andrade, D.; Marotta, L.; De Vasconcellos, R.; Chaves, I.; Carvalho, S.; Ferraz, L.; Penna, D.B.; Luzia, E.; Santos, D.S.; et al. Titanium–35niobium alloy as a potential material for biomedical implants: In vitro study. *Mater. Sci. Eng. C* **2015**, *56*, 538–544.
31. Hossain, S.S.; Roy, P.K. Study of physical and dielectric properties of bio-waste-derived synthetic wollastonite. *J. Asian Ceram. Soc.* **2018**, *6*, 289–298. [[CrossRef](#)]
32. Wang, H.; Zhang, Q.; Yang, H.; Sun, H. Synthesis and microwave dielectric properties of CaSiO₃ nanopowder by the sol-gel process. *Ceram. Int.* **2008**, *34*, 1405–1408. [[CrossRef](#)]
33. Kargarzadeh, H.; Sheltami, R.M.; Ahmad, I.; Abdullah, I.; Dufresne, A. Cellulose nanocrystal: A promising toughening agent for unsaturated polyester nanocomposite. *Polymer* **2015**, *56*, 346–357. [[CrossRef](#)]
34. Elimelech, M.; Zhu, X.; Childress, A.E.; Hong, S. Role of membrane surface morphology in colloidal fouling of cellulose acetate and composite aromatic polyamide reverse osmosis membranes. *J. Membr. Sci.* **1997**, *127*, 101–109. [[CrossRef](#)]
35. Paluszkiwicz, C.; Blazewicz, M.; Podporska, J.; Gumuła, T.; Paluszkiwicz, C.; Blaz, M. Nucleation of hydroxyapatite layer on wollastonite material surface: FTIR studies. *Vib. Spectrosc.* **2008**, *48*, 263–268. [[CrossRef](#)]
36. Huang, E.; Chen, C.H.; Huang, T.; Lin, E.H.; Xu, J.A. Raman spectroscopic characteristics of Mg-Fe-Ca pyroxenes. *Am. Mineral.* **2000**, *85*, 473–479. [[CrossRef](#)]
37. Izumi, C.M.S.; Temperini, M.L.A. Vibrational Spectroscopy FT-Raman investigation of biodegradable polymers: Poly (3-hydroxybutyrate) and poly (3-hydroxybutyrate-co-3-hydroxyvalerate). *Vib. Spectrosc.* **2010**, *54*, 127–132. [[CrossRef](#)]
38. Sun, Z.; Bai, Z.; Shen, H.; Zheng, S.; Frost, R.L. Electrical property and characterization of nano-SnO₂/wollastonite composite materials. *Mater. Res. Bull.* **2013**, *48*, 1013–1019. [[CrossRef](#)]
39. Olesov, B.A.K.; Eiger, C.A.G.; Kolesov, B.A.; Geiger, C.A. Behavior of H₂O molecules in the channels of natrolite and scolecite: A Raman and IR spectroscopic investigation of hydrous microporous silicates. *Am. Mineral.* **2006**, *91*, 1039–1048. [[CrossRef](#)]
40. Montanheiro, T.L.A.; Passador, F.R.; Oliveira, M.P.; Durán, N.; Lemes, A.P. Preparation and Characterization of Maleic Anhydride Grafted Poly(Hydroxybutyrate-CO-Hydroxyvalerate) -PHBV-g-MA. *Mater. Res.* **2016**, *19*, 229–235. [[CrossRef](#)]
41. Al-Abadleh, H.A.; Grassian, V.H. FT-IR study of water adsorption on aluminum oxide surfaces. *Langmuir* **2003**, *19*, 341–347. [[CrossRef](#)]

42. Lenza, R.F.S.S.; Nunes, E.H.M.M.; Vasconcelos, D.C.L.L.; Vasconcelos, W.L. Preparation of sol-gel silica samples modified with drying control chemical additives. *J. Non-Cryst. Solids* **2015**, *423*, 35–40. [[CrossRef](#)]
43. Bheemaneni, G.; Saravana, S.; Kandaswamy, R. Processing and Characterization of Poly (butylene adipate-co-terephthalate)/Wollastonite Biocomposites for Medical Applications. *Mater. Today Proc.* **2018**, *5*, 1807–1816. [[CrossRef](#)]
44. Wei, J.; Chen, F.; Shin, J.W.; Hong, H.; Dai, C.; Su, J.; Liu, C. Preparation and characterization of bioactive mesoporous wollastonite-Polycaprolactone composite scaffold. *Biomaterials* **2009**, *30*, 1080–1088. [[CrossRef](#)] [[PubMed](#)]
45. Cheng, W.; Li, H.; Chang, J. Fabrication and characterization of β -dicalcium silicate/poly (d, l-lactic acid) composite scaffolds. *Mater. Lett.* **2005**, *59*, 2214–2218. [[CrossRef](#)]
46. Alvares, L.; Tiago, R.; Bastos, M. Phenol removal from aqueous solution by carbon xerogel. *J. Sol-Gel Sci. Technol.* **2012**, *63*, 202–210.
47. Senturk, H.B.; Ozdes, D.; Gundogdu, A.; Duran, C.; Soylak, M. Removal of phenol from aqueous solutions by adsorption onto organomodified Tirebolu bentonite: Equilibrium, kinetic and thermodynamic study. *J. Hazard. Mater.* **2009**, *172*, 353–362. [[CrossRef](#)]
48. Salama, A.; Aljohani, H.A.; Shoueir, K.R. Oxidized cellulose reinforced silica gel: New hybrid for dye adsorption. *Mater. Lett.* **2018**, *230*, 293–296. [[CrossRef](#)]



© 2019 by the authors. Licensee MDPI, Basel, Switzerland. This article is an open access article distributed under the terms and conditions of the Creative Commons Attribution (CC BY) license (<http://creativecommons.org/licenses/by/4.0/>).